Design and Optimisation of a 2.4 GHz Radio-Frequency Energy Harvesting System for Low-Power Internet of Things (IoT) Applications

John Nyamekye Ansah., John Kojo Annan., Shiphrah Ohene Adu

Department of Electrical and Electronic Engineering, University of Mines and Technology, Tarkwa-Ghana

DOI: https://doi.org/10.51584/IJRIAS.2025.100900033

Received: 06 September 2025; Accepted: 12 September 2025; Published: 12 October 2025

ABSTRACT

This paper presents the design and performance evaluation of a highly efficient 2.4 GHz Radio-Frequency Energy Harvesting (RF-EH) system specifically modified to meet the energy requirements of low-power Internet of Things (IoT) applications. This system incorporates a high-gain 4x4 Microstrip Patch Antenna (MPA) Array, a single-stub Matching Network (MN) and a 5-stage RF-to-DC rectifier using the Cockcroft-Walton Voltage Multiplier (CW-VM) topology. The antenna is mounted on Rogers RT5880 substrate with a thickness of 1.588 mm and a relative permittivity of 2.2, and fed by a 50-Ω microstrip feed line. The antenna was designed using Computer Simulation Technology (CST) Studio Suite 2019, while the rectifier and MN were implemented in Keysight Advanced Design System (ADS) 2022. The antenna achieved a high gain of 19.29 dBi and a directivity of 20.01 dBi, with radiation and total efficiencies exceeding 84 %. The antenna demonstrated a highly directive E-Plane radiation pattern with a narrow beamwidth of 19.4° and a side lobe level of -13.8 dB, indicating a more focused reception of RF signals and a good suppression of unwanted radiation. The rectifier achieved a peak Power Conversion Efficiency (PCE) of 89.913 % and a peak output voltage of 16.424 V at an input power of 17.5 dBm. More importantly, low-input powers ranging from -20 dBm to 0 dBm produced usable DC output voltages from 0.456 V to 4.144 V, respectively, demonstrating strong suitability for IoT applications operating under limited RF conditions. These results demonstrated the system's potential for integration into large-scale indoor and outdoor IoT networks. The proposed system supports sustainable, maintenance-free and battery-less deployments, advancing the development of autonomous wireless systems.

Keywords: Radio-Frequency, Energy Harvesting, Antenna, Matching Network, Rectifier Circuit, IoT Applications

INTRODUCTION

The rapid proliferation of wireless sensors and Internet of Things (IoT) devices in recent times has intensified energy demand challenges. Most IoT nodes predominantly rely on battery power, necessitating frequent replacement and maintenance: an impractical and costly approach for large-scale or remote deployments. Their limited lifespan restricts scalability, while safety concerns, such as the risk of overheating and leakage, pose significant threats in industrial or high-temperature environments like agricultural farms and greenhouses [1].

Moreover, batteries contain toxic chemicals such as lead, lithium, and cobalt, which pose serious risks to the soil, aquatic life and human health if not properly disposed of. With IoT deployments expected to exceed 30 billion devices by 2030, the ecological consequences of large-scale battery use are projected to escalate. This points to the pressing need for a sustainable, eco-friendly and battery-less energy source to power IoT systems efficiently and at a low cost [2].

The realisation of autonomous and battery-less IoT systems can be effectively achieved through Energy Harvesting (EH) [3]. EH involves the collection of available ambient energy sources such as solar, thermal, wind, sound, vibration and Radio-Frequency (RF) signals. Among these, Radio-Frequency Energy Harvesting (RF-EH) offers a promising solution, primarily due to the global deployment of 5th Generation (5G) and ubiquity wireless infrastructure, such as mobile cell towers, Wi-Fi routers, FM radio and television (TV) transmitters.

ISSN No. 2454-6194 | DOI: 10.51584/IJRIAS |Volume X Issue IX September 2025

This persistent availability of RF energy makes it possible to harvest and convert ambient signals into usable power to drive low-power devices [4]. Hence, RF-EH presents a more favourable and sustainable solution for powering the next generation of wireless sensors and IoT devices [5].

The process of scavenging of electromagnetic (EM) energy from ambient RF bands is called RF-EH. RF-EH can be classified into near-field (NF) and far-field (FF) techniques, depending on propagation distance. Near-Field Energy Harvesting (NF-EH) transfers energy over short distances using inductive coupling, where coils generate a magnetic field to induce current. This technique is commonly used in wireless charging applications such as electric vehicles, smartphones and medical implants, but its efficiency decreases with increasing coil separation [6]. In contrast, Far-Field Energy Harvesting (FF-EH) employs antennas to intercept EM radiations which travel over long distances and is a widely adopted method for ambient RF-EH due to the ever-present availability of RF signals. However, FF-EH suffers from reduced input power density as a result of Free-Space Path Loss (FSPL), which increases with distance. Since it is impossible to capture all the transmitted RF power at the receiver end, improving RF-to-DC power conversion efficiency (PCE) under low input power conditions remains a key research challenge in RF-EH designs [7].

Model of Radio-Frequency Energy Harvesting System

A block diagram of the RF-EH system is presented in Figure 1. It consists of (a) a receiver antenna for collecting RF power from the target frequency band using the FF method; (b) a Matching Network (MN) to convey the received signal to a rectifier circuit by minimising reflection losses; (c) a rectifier circuit to convert the input alternating current (AC) signal into direct current (DC) signal and also acts as a voltage boosting block hence improving the output voltage at the end; (d) a DC pass filter to further remove higher order harmonics of AC signal which may escape rectification and (e) a DC-to-DC converter to maintain a stable DC output voltage irrespective of fluctuations in the input power or the load to serve low-power devices efficiently [8].

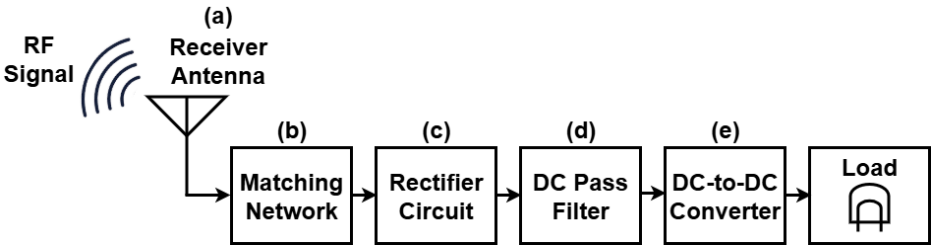

Figure 1. Block diagram of Radio-Frequency Energy Harvesting System

Recent studies have shown that RF signals are densely concentrated within the 1700-2650 MHz range, covering numerous communication bands, such as GSM-1800 (1805-1880 MHz), UMTS (1930-1990 MHz) (2110-2170 MHz), Wi-Fi/Bluetooth (2400-2483.5 MHz) and LTE-2600 (2620-2690 MHz). Hence, a substantial amount of RF energy is available within these bands, which can be effectively captured and converted into a usable DC signal [8].

However, since RF power density decreases with increasing propagation distance, the received signal is usually weak at the harvesting node. Therefore, an RF-EH system needs to employ a high-efficient antenna for effective energy capture, a well-optimised MN to maximise power transfer (PT) to the rectifier and a high-performance rectifier with enhanced PCE and DC output voltage. These components collectively ensure the sustainable operation of low-power IoT devices while minimising the reliance on standard batteries [7].

Receiver Antenna

The antenna acts as the initial interface between ambient RF signals and the EH circuitry. Single-band antennas achieve high efficiency at a specific frequency but fail when the target frequency is unavailable, leading to weak received input power. Broadband antennas can harvest energy across a wide frequency range but suffer from low efficiency. Multi-band antennas, on the other hand, provide a balanced solution by targeting selected frequencies, thus improving both efficiency and output power. Antennas may also be directional or omnidirectional: directional antennas offer high gain and efficient energy capture from fixed RF sources, but

ISSN No. 2454-6194 | DOI: 10.51584/IJRIAS |Volume X Issue IX September 2025

require precise alignment, whereas, omnidirectional antennas, though lower in gain, are mostly preferred when the direction of incoming signals is unknown [9].

The Microstrip Patch Antenna (MPA) is widely used in wireless communication and RF-EH, due to its compactness, lightweight, low cost, robustness and ease of fabrication using printed circuit technology. However, despite the suitability of MPAs for RF-EH, they suffer from several limitations when implemented as a single-patch antenna. These include low efficiency, narrow bandwidth, spurious radiation, poor power-handling capacity and low gain [7].

Matching Network

In the RF-EH system, frequent high impedance variations often arise from the non-linear behaviour of rectifier components such as diodes or transistors [5]. To minimise reflection losses and enhance PT between the antenna and the rectifier, a Matching Network is introduced. MNs can be realised using either lumped elements or distributed elements. Lumped-Element Matching Networks (LE-MNs) use passive components like inductors, capacitors, resistors and transformers. Commonly used topologies include L-matching, Pi (π)-matching and T-matching networks, which are effective at low frequencies (< 500 MHz), where component dimensions remain small relative to the signal wavelength.

At high frequencies (> 500 MHz), Distributed-Element Matching Networks (DE-MNs) are preferred since lumped elements become impractical due to parasitic effects and difficulties in achieving precise capacitance or inductance values. They employ transmission line (TL) sections such as microstrip lines or coplanar waveguides to perform impedance matching (IM). DE-MNs are primarily classified into three types: quarter-wave transformers, stub (single or double) MNs and multi-section TL transformers. In DE-MNs, impedance transformation (IT) is achieved by adjusting the length and width of the TL sections [10].

Rectifier Circuit

The rectifier circuit is a key component of RF-EH systems, converting weak AC signals from the MN into DC signals and boosting it to provide a sufficient output. Rectifiers are generally classified as half-wave or full-wave. Half-wave rectifiers, consisting of a single diode connected in series or parallel with the output load, are simple and low-cost but suffer from high voltage ripple and poor PCE, making them unsuitable for sensitive applications. Full-wave rectifiers are classified as Dickson Charge Pump (DCP), Cockcroft-Walton (CW) and Cross-Coupled Differential-Drive (CCDD) rectifiers. A single-stage CW rectifier is also called a Greinacher Voltage Doubler (GVD). Among the common voltage multiplier (VM) topologies, the CW multiplier is well-suited for low-power applications that require a high DC output. Its simple, passive, scalable and clock-free architecture allows for easy addition of multiple stages to increase the output voltage under low input power conditions. Unlike DCP, which requires clock signals, or CCDD, which suffers from scalability and layout sensitivity, the CW rectifier remains the preferred choice for RF-EH systems [5, 10].

In conclusion, RF-EH offers a promising approach toward autonomous, battery-less IoT systems by leveraging ambient RF energy and optimising key components such as antennas, MNs and rectifiers. This approach may significantly reduce dependence on conventional batteries, lowering cost and supporting sustainability.

LITERATURE REVIEW

Significant research work has been done on RF-EH systems operating at the Industrial Scientific and Medical (ISM) band. The authors in [8] presented a small dual-band antenna with gains of 1.6 dBi and 3.95 dBi at 2.4 GHz and 5.2 GHz, respectively. The two-ring resonators reported in [3] measured a peak gain of about 5 dBi between 1.68-2.80 GHz, with a 50 % fractional bandwidth. A dual-band MPA was reported in [9]. It achieved low gains of 0.5102 dBi and 1.175 dBi, with poor radiation efficiencies at 2.4 GHz and 5.8 GHz, respectively. Three models of MPA comprising 1x1, 2x2 and 4x4 were reported in [12]. The 4x4 model recorded the highest gain of 13.05 dBi, operating effectively within 2.32-2.40 GHz. However, its large physical size poses integration challenges in miniaturised systems. The antenna proposed in [13] was optimised using machine learning algorithms to reduce simulation time and accelerate the design process. The antenna with omnidirectional

ISSN No. 2454-6194 | DOI: 10.51584/IJRIAS |Volume X Issue IX September 2025

radiation properties operated effectively between 1.72-3.02 GHz and 3.47-4.79 GHz, covering mobile frequency and Wireless Local Area Network (WLAN) bands. The authors in [14] presented a 2x2 MPA array to harness mobile frequency signals from the GSM-1800 band. It achieved a gain of 9.2 dBi with a good return loss value of -25 dB. Four models of triangular MPA arrays comprising 1x2, 2x2, 2x3 and 2x4 were designed in [15]. The 2x2 model outperformed both the 2x3 and 2x4 arrays with a gain of 11 dBi, even though it had fewer patch elements. A three-element patch array was presented in [7] for RF-EH. It measured a gain of 11.24 dBi with radiation and total efficiencies exceeding 89 %. The authors in [16] proposed a seven-element MPA array with a gain of 15.8 dBi. The 2.4 GHz MPA array reported in [17] achieved a gain of 17.5 dBi.

A 2.45 GHz compact-sized rectenna (antenna + rectifier) was reported in [18]. The system employed an L-type MN and single-stage GVD, all fabricated on an FR-4 substrate. The rectifier comprised a pair of HSMS-2850 Schottky diodes chosen for their low turn-on voltage and fast switching speed at high frequencies. The antenna achieved a gain of 1.3 dBi, while the output voltage and PCE of the rectifier recorded 2.9 V and 75 %, respectively, at 10 dBm. The single-stage RF-to-DC converter presented in [6] achieved an output voltage of 21 mV at -18 dBm. The rectenna proposed in [19] comprised a 2x1 array antenna with an L-type MN selected for compactness. A rectenna operating at 2.45 GHz was proposed in [20] for RF-EH applications. The design recorded a gain of 7.31 dBi, with maximum output voltage and PCE of 5.2 V and 64 % respectively, at 0 dBm. The rectenna proposed in [21] comprised a 1x2 MPA and a seven-stage CW rectifier with an L-type MN. The antenna achieved a gain of 7.03 dBi with an output voltage of 12 V and PCE of 75 % at 20 dBm.

Previously reported RF-EH designs face significant challenges, notably low antenna gain [3, 8, 9, 13, 18] and poor radiation efficiency [12, 14, 15, 17], both of which hinder effective RF signal capture in dynamic or low-signal environments. Although L-type MN is widely adopted for its simple structure, low insertion loss and high efficiency at a single frequency [18-21], it remains impractical at high frequencies [10]. Furthermore, only a few RF-EH systems have employed multi-stage rectifiers, which are essential for boosting output voltage to meet the demands of low-power devices [20-21]. Consequently, the review recommends that advanced RF-EH systems incorporate high-gain antennas, optimised MNs using distributed elements and multi-stage rectifiers to achieve sufficient output voltage and improve PCE.

This research proposes the design and optimisation of a 2.4 GHz RF-EH system for low-power IoT applications. The system integrates a high-gain 4x4 MPA array for efficient RF signal capture and a 5-stage CW rectifier with a single-stub MN. The multi-stage topology is employed to maximise the DC output voltage and PCE, thereby improving the system's reliability to meet the energy demands of low-power IoT devices. The single-stub MN was also utilised to minimise signal reflection and ensure maximum PT between the antenna and the rectifier.

The remainder of this paper is organised as follows. The materials and methods used are presented in Section 2. Followed by results and discussion in Section 3 and the conclusion in Section 4.

MATERIALS AND METHODS USED

Receiver Antenna Design

Single-Element Patch Antenna

Figure 2 shows the design of a single-element (1x1) patch antenna, which served as a template for developing the 4x4 MPA array. The antenna was mounted on Rogers RT5880 substrate (dielectric constant = 2.2, loss tangent = 0.0009, height = 1.588 mm). Both the patch and the ground plane were made of annealed copper with a thickness of 0.035 mm, and the total area of the antenna was 90 × 100 mm². Rogers RT5880 substrate was selected for its low dielectric constant and loss tangent, which provides better IM, reduced signal loss and a more precise radiation pattern, making it suitable for high-frequency applications. Annealed copper was chosen for its excellent conductivity and minimal resistive losses.

A 50 Ω microstrip feed line (length Lf = 22.84 mm, width Wf = 4.89 mm) was used to feed the antenna with optimal power for normal operation, while a full ground plane ensured improved directivity and reduced back-lobe radiation. Both the ground plane and substrate shared the same dimensions (Lg = Ls = 90 mm, Wg = Ws =

ISSN No. 2454-6194 | DOI: 10.51584/IJRIAS |Volume X Issue IX September 2025

100 mm). A recessed distance of length Lif = 9.16 mm and a feed gap of width Wif = 9 mm were cut into the patch to ensure that the antenna resonates at 2.4 GHz with excellent IM. The antenna dimensions were derived from the standard design equations provided below:

Patch width:

$$Wp = \frac{c}{2f_o}\sqrt{\frac{2}{\varepsilon_r + 1}} \quad (1)$$

where, Wp = patch width

c = speed of light in a vacuum

fo = resonant frequency

εr = dielectric constant of the substrate

Patch length:

$$\varepsilon_{reff} = \frac{\varepsilon_r + 1}{2} + \frac{\varepsilon_r - 1}{2\sqrt{1 + 12\left(\frac{h}{Wp}\right)}} \quad (2)$$

$$\Delta Lp = 0.412h\left(\frac{\varepsilon_{reff} + 0.3}{\varepsilon_{reff} - 0.258}\right)\left(\frac{\frac{Wp}{h} + 0.264}{\frac{Wp}{h} + 0.8}\right) \quad (3)$$

$$Lp_{eff} = \frac{c}{2f_o\sqrt{\varepsilon_{reff}}} \quad (4)$$

$$Lp = Lp_{eff} - 2\Delta Lp \quad (5)$$

where, εreff = effective dielectric constant

h = substrate height

Lp = actual length of patch

ΔLp = extension of patch length

Lpeff = effective patch length

Substrate length and width:

$$Ls = Lp + 6h \quad (6)$$

$$Ws = Wp + 6h \quad (7)$$

where, Ls = Length of the substrate

Ws = Width of the substrate

Feed line length and width:

$$Lf = 0.25\lambda_g \quad (8)$$

ISSN No. 2454-6194 | DOI: 10.51584/IJRIAS |Volume X Issue IX September 2025

$$\lambda_g = \frac{\lambda_o}{\sqrt{\varepsilon_{reff}}} \quad (9)$$

$$\lambda_o = \frac{c}{f_o} \quad (10)$$

$$Wf = \frac{7.48h}{e^{\left(\frac{Z_o\sqrt{\varepsilon_r}+1.41}{87}\right)}} - 1.25t_t \quad (11)$$

where, Lf = length of the feed line

λg = guided wavelength

λo = wavelength of the resonating frequency

Wf = width of the feed line

Zo = impedance of the feed line

tt = trace thickness

***Recessed distance*:**

$$Lif = \frac{Lp}{\pi}\cos^{-1}\left(\sqrt{\frac{Z_o}{Z_{in}}}\right) \quad (12)$$

where, Lif = recessed distance

Lp = length of the patch

Zo = characteristic impedance of the microstrip feed line

Zin = input impedance of the patch edge

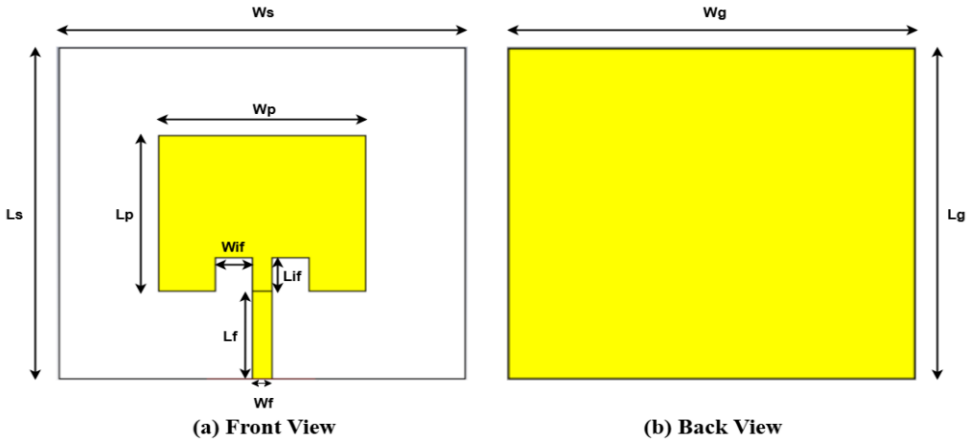

Figure 2. Design of Single-Element (1x1) Patch Antenna

Proposed 4x4 Microstrip Patch Antenna Array

Figure 3 shows the design of the proposed 4x4 MPA array, which was created by arranging four 1x4 linear arrays in parallel and feeding them from a single feed point. The array was mounted on a full ground plane of the same area as the dielectric substrate. A 50 Ω microstrip feed line was first created along one of the edges of the substrate extending towards the centre. The feed line dimensions were length Lmf = 200 mm and width Wmf = 4.89 mm and served as the main feed to the identical patch elements. A T-junction (tj) feed line was created at

ISSN No. 2454-6194 | DOI: 10.51584/IJRIAS |Volume X Issue IX September 2025

the end of the main feed line to divide the power coming from the main feed line equally among four sub-arrays consisting of four patch elements each. This T-junction is labelled (tj_4). This tj_4 feed line was connected to tj_3 via a pair of quarter-wave transformer (QwT) lines (Q_4) and the connector (C_4) at both ends. Tj_3 further splits and conveys power equally to two pairs of patch elements within each sub-array through Q_3 and C_3. At the ends of C_3, the power is again equally divided using Tj_2 through Q_2 and C_2, leading to Tj_1. Finally, at Tj_1, power is distributed equally to each patch element through dedicated patch feed lines. The physical dimensions of the 4x4 MPA array are provided in Appendix A.

The addition of more patch elements were adopted to enhance directivity and gain by receiving more power in a specified direction. Moreover, careful arrangement of identical patch elements, with controlled amplitudes and phases, improves radiation efficiency and shapes the overall radiation pattern.

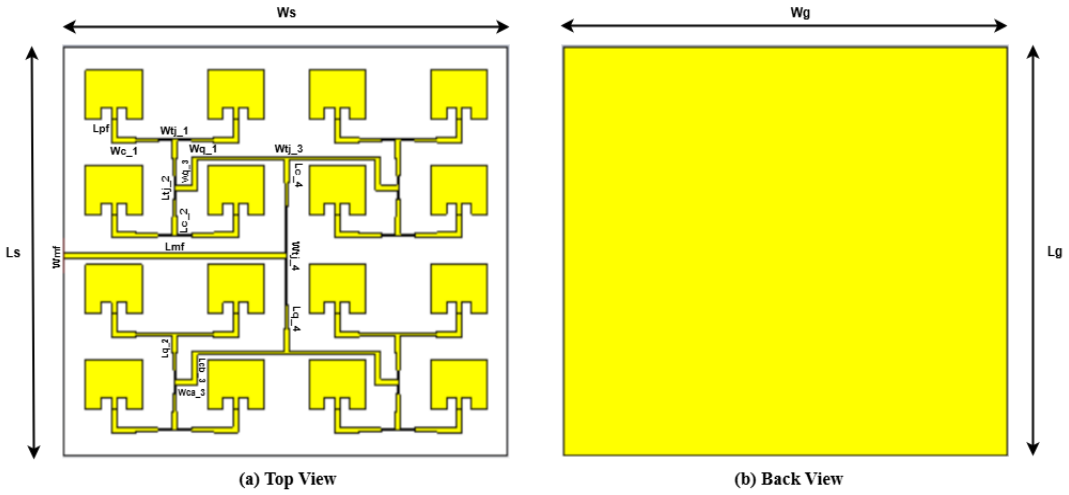

Figure 3. Design of 4x4 Microstrip Patch Antenna Array

Matching Network Design

The design of a MN is to ensure maximum PT between the antenna and the rectifier circuit. This is achieved by transforming the complex impedance of the rectifier to match the characteristic impedance of the antenna, which is usually 50 Ω. A 5-stage CW rectifier was first designed, and its input impedance was measured by plotting Zin against frequency. At 2.4 GHz, the rectifier input impedance was obtained as (3.815 – j37.583) Ω, which served as a reference for designing the MN.

Owing to the degraded performance of lumped elements at high frequencies, a single-stub MN based on microstrip TLs was adopted for a more practical and high-performance design. An ideal TL model was designed using the Smith Chart Utility (SCU) in ADS to transform the rectifier impedance to 50 Ω. The impedances and electrical lengths of the ideal TLs were obtained as (50 Ω, 13.09°) for TL1 and (50 Ω, 24.56°) for TL2, as shown in Figure 4. These values serve as initial design parameters for further implementation using microstrip lines and subsequent optimisation. TL1 and TL2 represent a short-circuit stub (SCS) and a series microstrip line (SML), respectively.

For practical implementation, the ideal TLs were converted to real microstrip lines. This process began by defining the substrate on which the microstrip lines would be etched. The MSub component was selected from the component palette, and its parameters were entered. Rogers RT5880 was selected as the substrate, consistent with the antenna substrate, to maintain impedance continuity and minimise parasitic effects. The LineCalc option in the Tools menu was used to convert the ideal TL parameters into their corresponding physical dimensions (length and width) based on the defined substrate properties. The resulting single-stub MN consisted of the following components: TL3, TL5, MTEE and MLSC.

Simulation of the initial layout produced an S11 value of -1.866 dB at 2.4 GHz, indicating sub-optimal IM. To enhance performance, optimisation of the TL dimensions was performed. The widths of all the TLs were fixed at 4.89 mm to match the antenna feed line, while the length of TL5 was set to 2 mm. Prior to optimisation, the

ISSN No. 2454-6194 | DOI: 10.51584/IJRIAS |Volume X Issue IX September 2025

stub length (Lc) and SML length (Ld) were obtained as 3.31 mm and 6.21 mm, respectively. An optimisation goal of S11 < -60 dB at 2.4 GHz was defined, with Lc and Ld varied between 1 mm and 20 mm. The Quasi-Newton (QN) algorithm was employed with 100 iterations and a target error of 0.00001. Following optimisation, the MN demonstrated significantly improved matching characteristics. Figure 5 presents the single-stub MN for the 5-stage CW rectifier after optimisation.

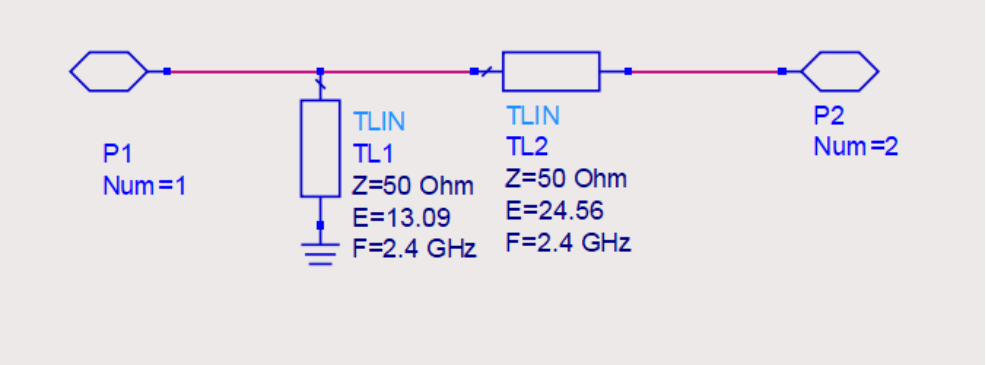

Figure 4. Ideal Transmission Line Model of Single-Stub Matching Network

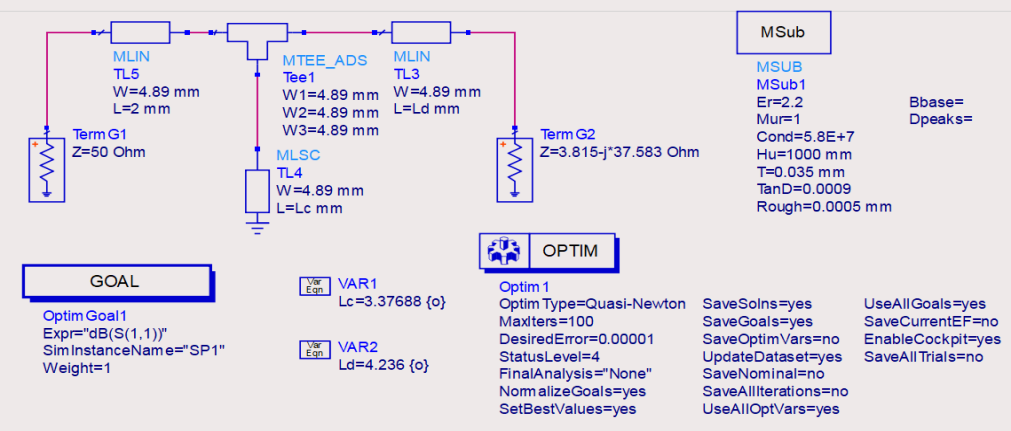

Figure 5. Single-Stub Matching Network for 5-Stage CW Rectifier After Optimisation

Rectifier Circuit Design

The rectifier converts harvested RF energy from the antenna into usable DC output. In this research, a 5-stage rectifier based on the Cockcroft-Walton Voltage Multiplier (CW-VM) topology was implemented to achieve high PCE and appreciable DC output voltage under low input power conditions. Each stage of the CW rectifier consists of two Schottky diodes and a pair of capacitors. Zero-bias HSMS-2850 Schottky diodes were chosen for their low turn-on voltage (150-250 mV) and fast switching performance at high frequencies, making them suitable for RF-EH applications. The utilisation of Schottky diodes ensures minimal voltage loss during rectification, resulting in improved PCE, while the capacitors in the circuit store and transfer charge between stages, enabling voltage multiplication.

The circuit model of the zero-bias Schottky diode is illustrated in Figure 6. It consists of a 0.7 nH series inductor and a 0.25 pF shunt capacitor to account for parasitic effects arising from the diode's bond wires, package leads and stray capacitance. Model parameters (DIODEM1), derived from the manufacturer's data sheet, ensured accuracy during Harmonic Balance (HB) simulations [21]. These parameters are displayed in Table 1.

The schematic diagram of the 5-stage CW rectifier is presented in Figure 7. A custom diode model symbol was created from the HSMS-2850 model and reused across subsequent stages. A separate schematic was then designed to determine the optimal load resistance and input RF power that maximises the rectifier's PCE, as

well as the input impedance associated with these values. This new schematic implemented a 5-stage CW-VM

ISSN No. 2454-6194 | DOI: 10.51584/IJRIAS |Volume X Issue IX September 2025

topology having two of the custom-defined diode models and a pair of 150 pF series capacitors for each stage with a 0.047 pF shunt capacitor at the output to act as a low-pass filter.

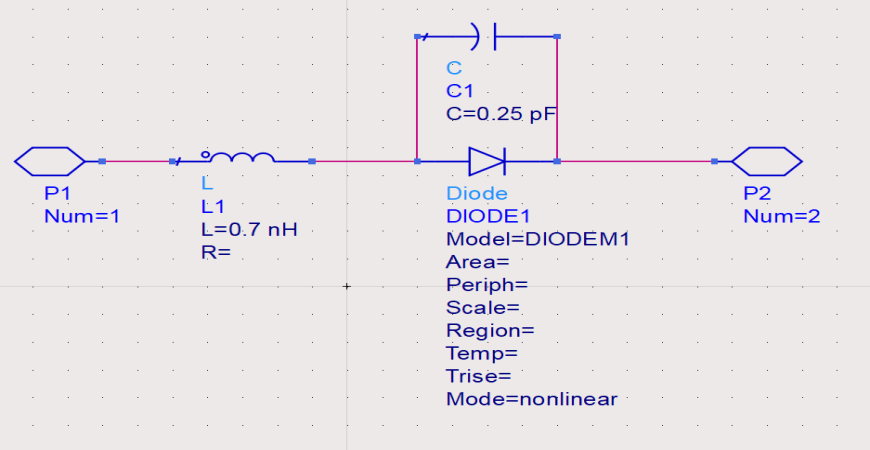

Figure 6. Circuit Model of Zero-Bias Schottky Diode

Table 1. Parameters of Zero-Bias HSMS-2850 Schottky Diode

Parameter	**Value**	**Unit**
Minimum forward voltage	0.15	V
Saturation current	3	µA
Saturation maximum reverse leakage current	150	µA
Breakdown voltage	3.75	V
Parasitic series resistance	25	Ω
Junction capacitance	0.18	pF
Detection sensitivity	50	mV/µW

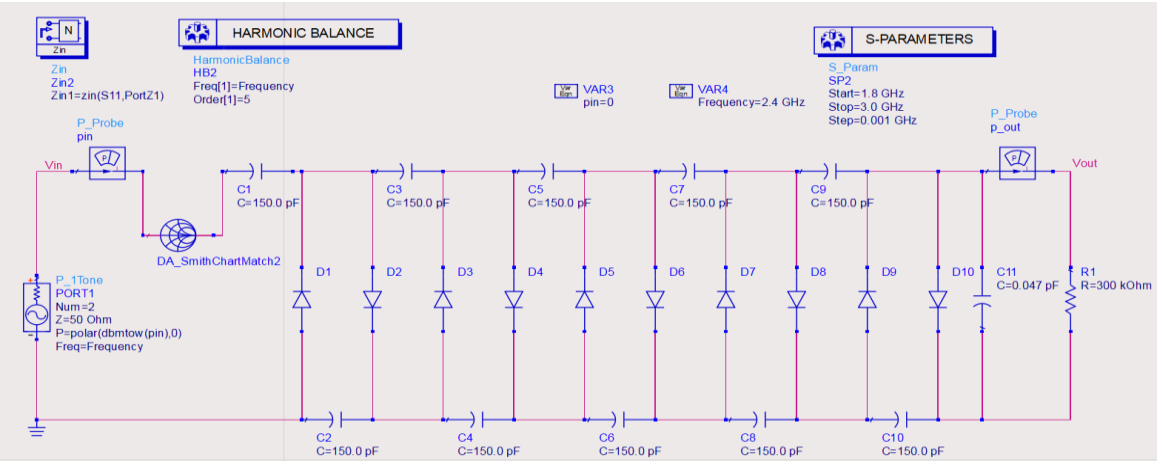

Figure 7. Schematic Diagram of Proposed 5-Stage CW Rectifier

The rectifier was driven by a single-tone RF source (P_1Tone) at 2.4 GHz with a characteristic impedance of 50 Ω. Input power was controlled by the variable pin (in dBm), allowing for flexible power sweep analysis. An HB analyser was used to model nonlinear diode behaviour, with harmonics up to the fifth order (Order[1] = 5) considered to capture rectification dynamics and harmonic content.

Initial simulations were performed without the MN, and the input impedance of the rectifier was obtained as (3.815 – j37.583) Ω. To match the rectifier's input impedance with the 50 Ω source, a single-stub MN was designed using the Smith Chart Tool in ADS. S-parameter simulation results confirmed that the MN successfully transformed the source impedance to match the rectifier's input impedance at 2.4 GHz. With the MN (DA_SmithChartMatch2) integrated, the rectifier demonstrated significant improvements in both output DC voltage and PCE. Optimal performance was observed with a 300 kΩ load resistance, where cascaded stages combined with precise IM substantially enhanced rectification efficiency.

RESULTS AND DISCUSSION

Antenna Performance

The return loss represents the portion of incident power reflected due to impedance mismatch between the antenna and its feedline. For effective operation, values below -10 dB are required. As shown in Figure 8, both antennas achieve return loss values below -25 dB at 2.4 GHz: -33.204 dB for the 1x1 patch and -25.56 dB for the 4x4 array. The slightly less negative value of the 4x4 array is attributed to the complexity of its feed structure and mutual coupling effects of adjacent array elements [7]. The measured bandwidths were 41.4 MHz (2.3793 – 2.4207 GHz) for the 1x1 patch and 33.5 MHz (2.3843 – 2.4178 GHz) for the 4x4 array, both sufficient for ISM-band operation. The Voltage Signal Wave Ratio (VSWR) is also an important parameter that specifies how well the antenna is matched with its feedline. A VSWR between 1 and 2 indicate acceptable matching [11]. As shown in Figure 9, the 1x1 patch and the 4x4 array achieved 1.0447 and 1.1113, respectively, both close to unity, confirming minimal reflection losses.

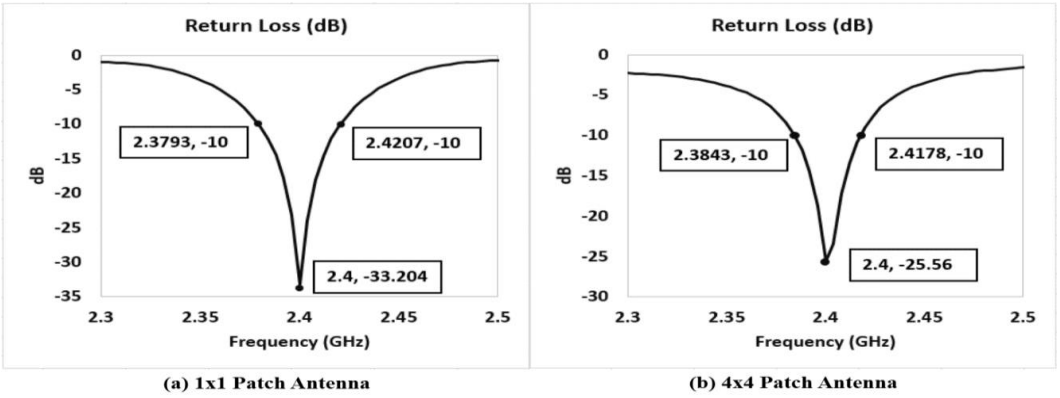

(a) 1x1 Patch Antenna (b) 4x4 Patch Antenna

Figure 8. Return Loss

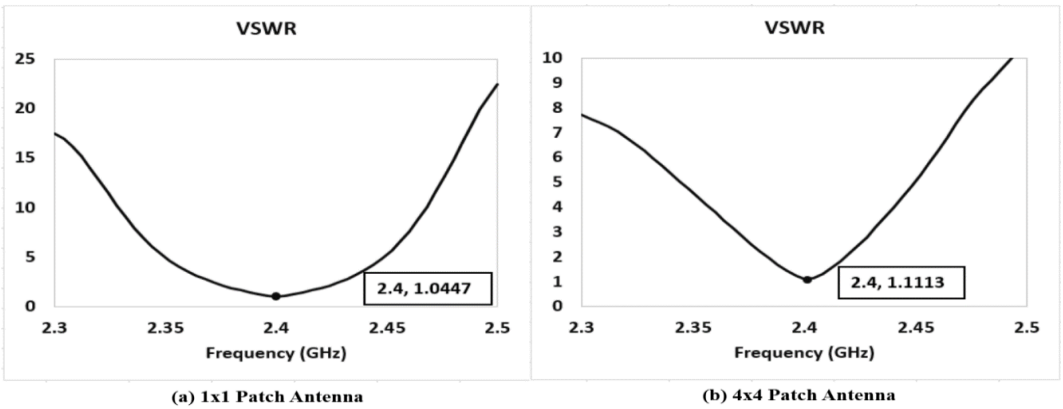

(a) 1x1 Patch Antenna (b) 4x4 Patch Antenna

Figure 9. VSWR

Figure 10 shows that the 1x1 patch achieved a gain of 7.122 dBi, which increased to 19.29 dBi with the 4x4 array due to its large aperture and constructive interference of EM waves from multiple, closely spaced elements. Directivity also improved, from 8.081 dBi for the 1x1 patch to 20.01 dBi for the 4x4 array as seen in Figure 11. The measured radiation efficiencies were -0.9586 dB (80.19 %) for the 1x1 patch and -0.7218 dB (84.69 %) for

ISSN No. 2454-6194 | DOI: 10.51584/IJRIAS |Volume X Issue IX September 2025

the 4x4 array, while total efficiencies were -0.9712 dB (79.96 %) and -0.7346 dB (84.44 %), respectively. Despite coupling losses, the 4x4 array achieved over 84 % of total and radiation efficiencies, meeting RF-EH requirements. Efficiency in percentage was determined using equation (13):

$$\text{Efficiency (\%)} = 10^{0.1 \times (\text{Rad or Tot Efficiency}) \text{ dB}} \quad (13)$$

where, Efficiency (%) = Efficiency in percentage

(Rad or Tot Efficiency) dB = Radiation or Total Efficiency in dB

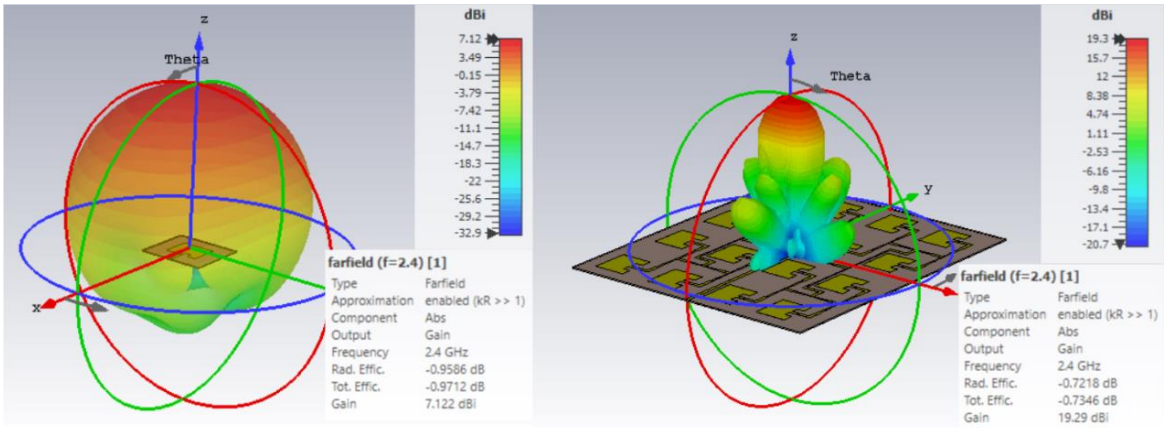

(a) 1x1 Patch Antenna **(b) 4x4 Patch Antenna**

Figure 10. 3D Gain Plot

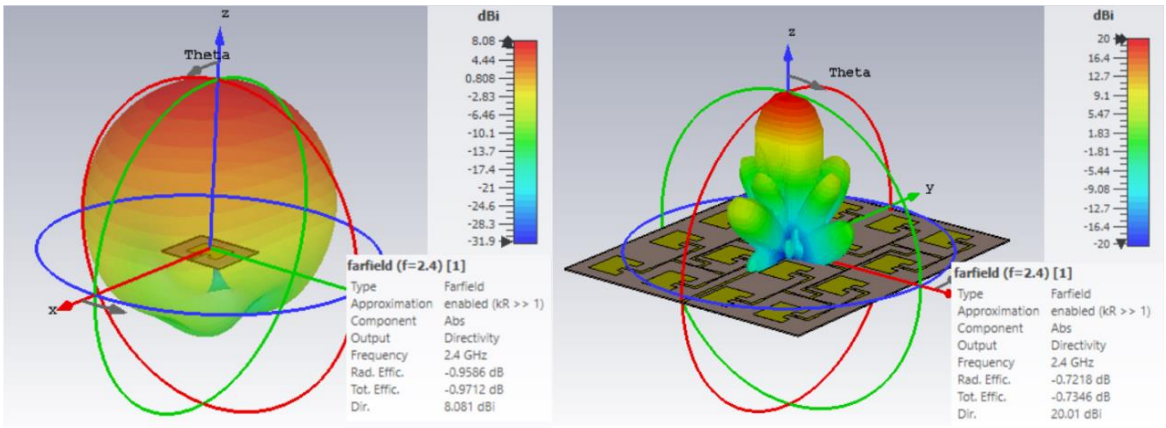

(a) 1x1 Patch Antenna **(b) 4x4 Patch Antenna**

Figure 11. 3D Directivity Plot

The E-plane radiation pattern (φ = 0°) shows the elevation-plane behaviour. As shown in Figure 12, the 1x1 patch exhibited a main lobe magnitude of 7.14 dBi at 2°, with a 77.2° beamwidth and a -19.2 dB side lobe. The 4x4 array produced a narrower 19.4° beamwidth, a 19.3 dBi main lobe at 0° and a -13.8 dB side lobe, corresponding to only 4.2 % power loss into undesired directions. The H-plane radiation pattern (φ = 90°) exhibits similar improvements as seen in Figure 13. The 1x1 patch achieved 7.12 dBi with a 70.9° beamwidth and -20.8 dB side lobe, while the 4x4 array reached 19.3 dBi with a 15.9° beamwidth and -12.9 dB side lobe.

Overall, the 4x4 array demonstrated superior gain, directivity, radiation and total efficiencies, and highly focused E and H plane patterns, confirming its suitability for efficient RF-EH.

ISSN No. 2454-6194 | DOI: 10.51584/IJRIAS |Volume X Issue IX September 2025

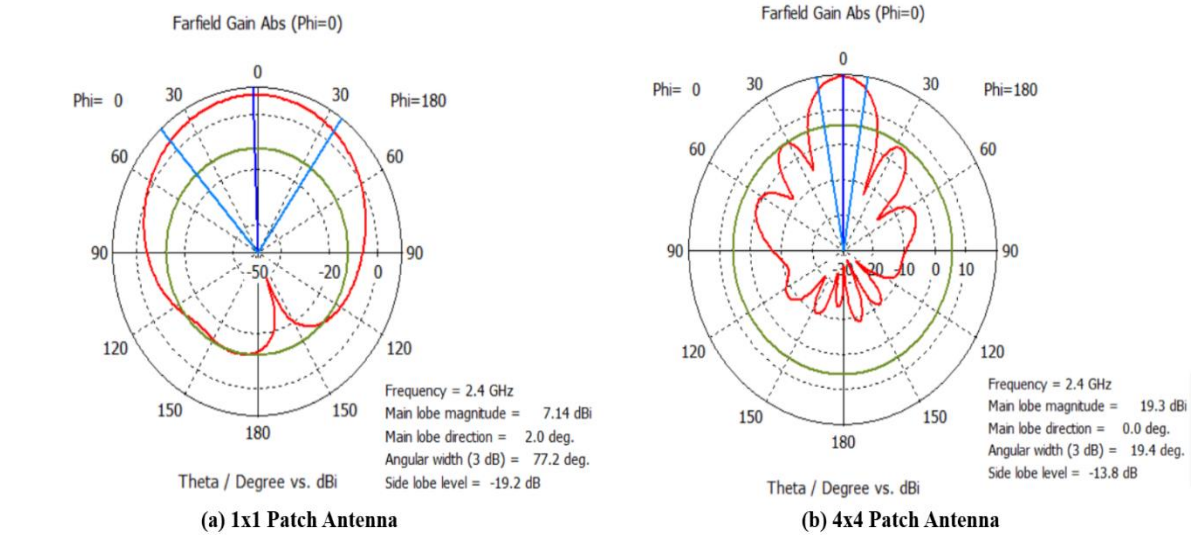

(a) 1x1 Patch Antenna (b) 4x4 Patch Antenna

Figure 12. E-Plane Radiation Pattern

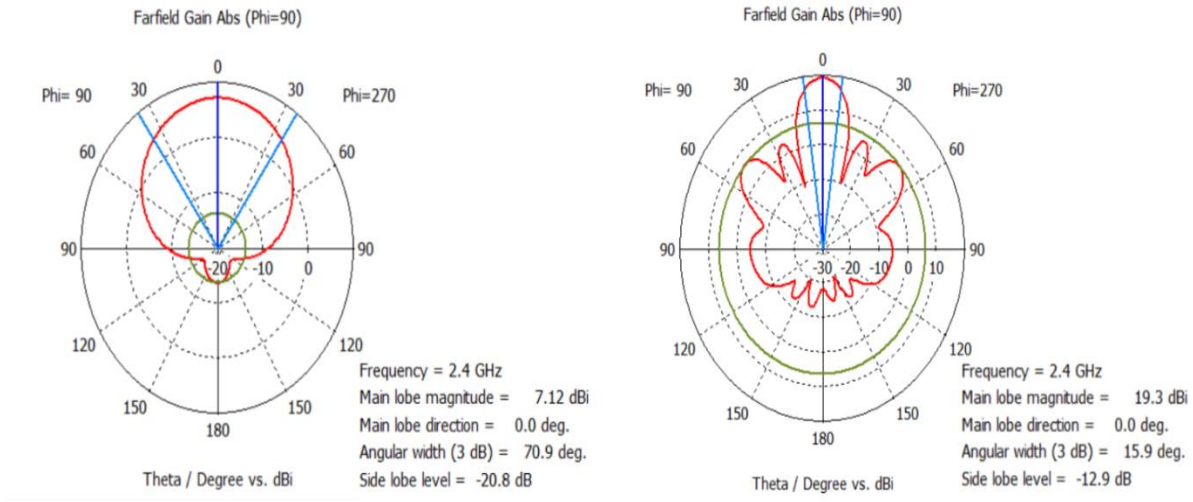

(a) 1x1 Patch Antenna (b) 4x4 Patch Antenna

Figure 13. H-Plane Radiation Pattern

Matching Network Performance

Figure 14 illustrates the return losses of the single-stub MN for the 5-stage CW rectifier before and after optimisation. Using the QN algorithm, the physical dimensions of the SCS stub and SML were adjusted for optimal IM at 2.4 GHz. The initial return loss was -1.866 dB, indicating poor matching. After optimisation, it improved significantly, to -62.858 dB. The QN algorithm gave a final value of -62.8599 dB within only five iterations, demonstrating higher accuracy and efficiency. The optimised lengths were Lc = 3.37688 mm and Ld = 4.236 mm for SCS and SML, respectively, as shown in Figure 15. These refinements fine-tuned the MN for maximum PT to the rectifier. These results confirm the precision advantage of QN over alternative ADS optimisation methods, which explains why it is commonly used for single-frequency S11 parameter optimisation.

Figure 16 presents the real and imaginary components of the 5-stage CW rectifier before and after matching. At 2.4 GHz, the input impedance was (3.815 – j37.583) Ω, indicating severe mismatch. After integrating the single-stub MN, the impedance transformed to (50.221 – j0.052) Ω, where the real part closely approached 50 Ω and the imaginary part nearly cancelled out, signifying successful IT. Figure 17 illustrates the return loss, which improved from -0.847 dB (unmatched) to -52.907 dB (matched). The results demonstrate a near-perfect IM, with minimal power loss between the rectifier and the 50 Ω RF source. The single-stub MN therefore proves effective and reliable for integration into the cascaded 5-stage rectifier circuit.

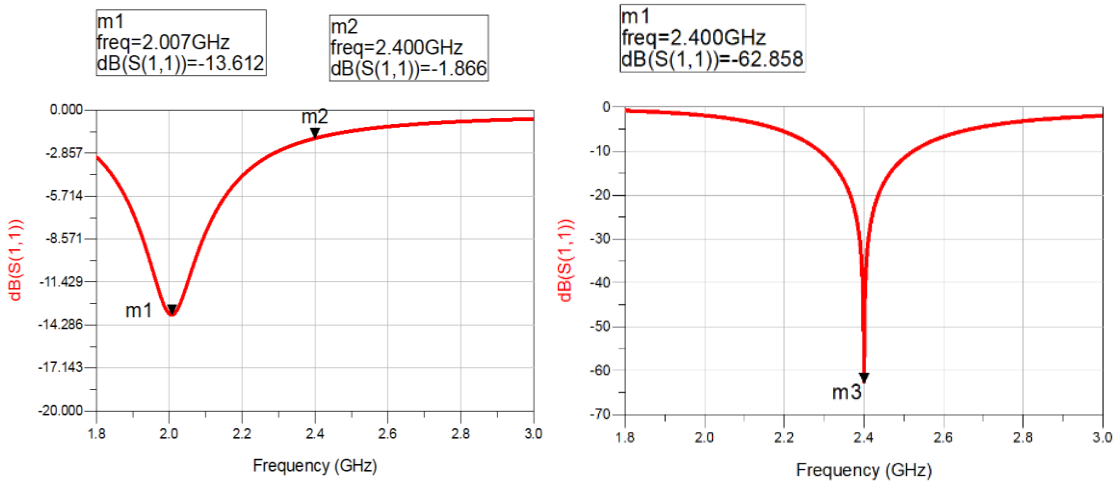

(a) Before Optimisation **(b) After Optimisation**

Figure 14. Return Loss of Single-Stub MN

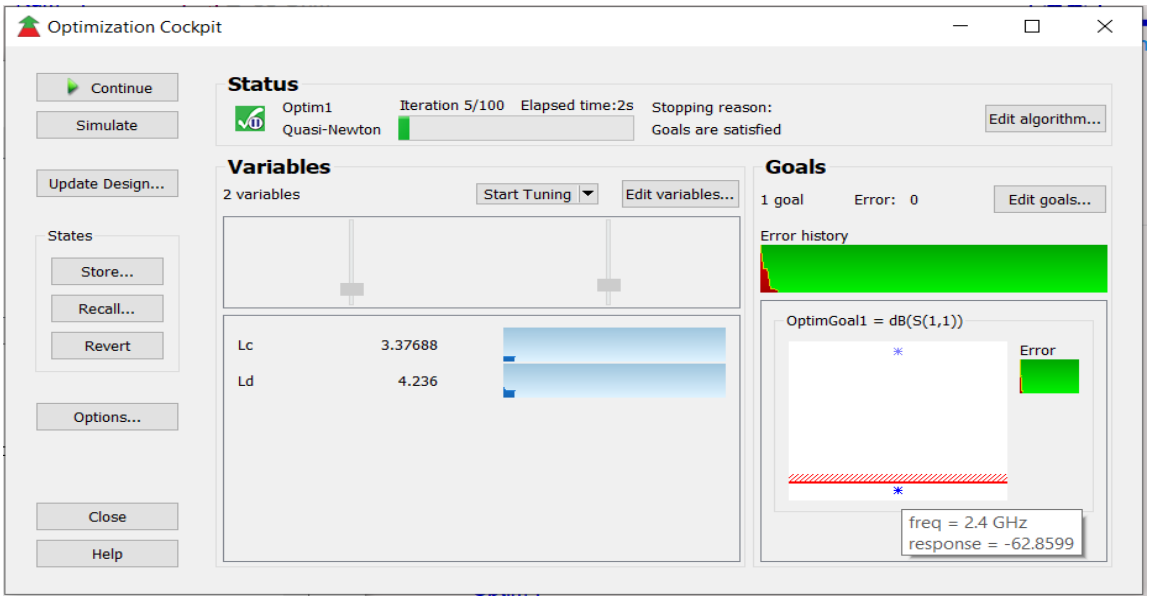

Figure 15. Optimised Dimensions of Single-Stub MN using Quasi-Newton Algorithm

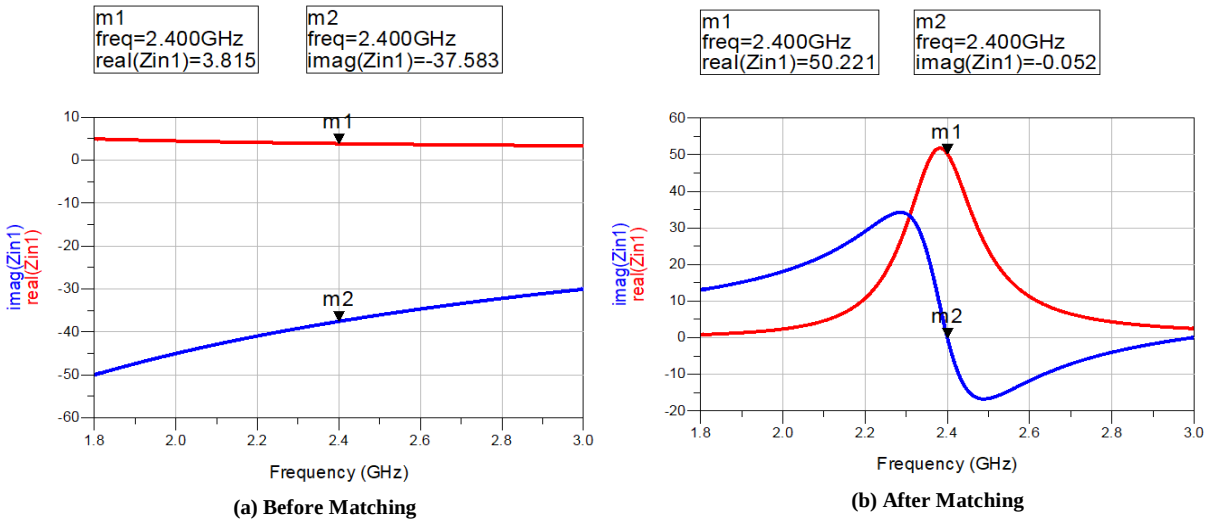

(a) Before Matching **(b) After Matching**

Figure 16. Input Impedance of 5-Stage CW Rectifier

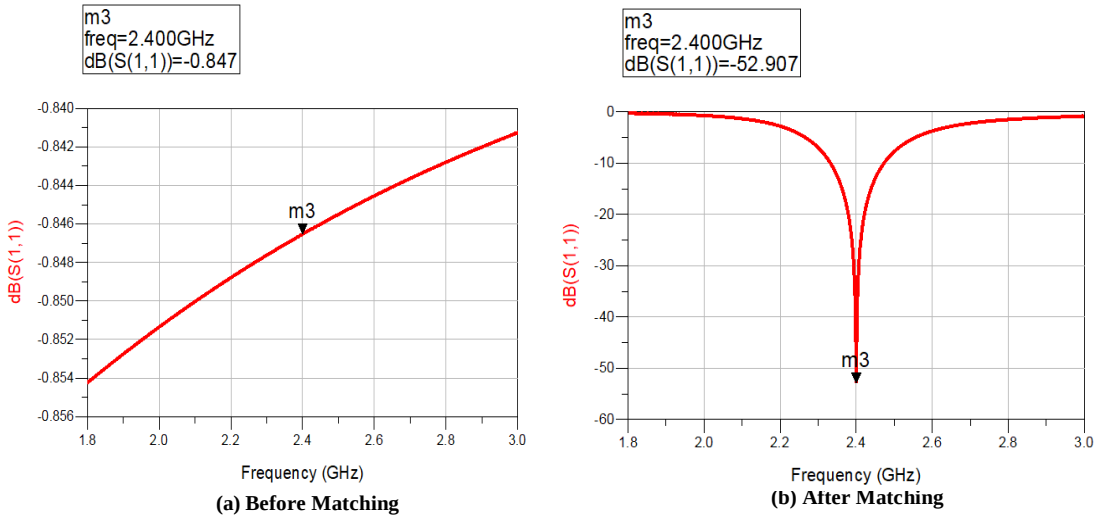

Figure 17. Return Loss of 5-Stage CW Rectifier

Rectifier Performance

Figure 18 shows the variation of input power (Pin) with output DC voltage for the proposed 5-stage CW rectifier. The circuit exhibits a steady increase in output voltage across the measured Pin range, beginning with 0.456 V at -20 dBm, which corresponds to extremely weak input RF signals typically observed in ambient IoT environments. At -10 dBm, the output DC voltage rises to 1.670 V, while at 0 dBm it achieves 4.144 V, demonstrating its capability to harvest sufficient energy for low-power sensing applications. A further increase to 10 dBm results in 9.816 V, and the maximum recorded output is 16.424 V at 17.5 dBm.

Figure 19 presents the rectifier's PCE as a function of Pin. The efficiency improves gradually, starting from 0.069 % at -20 dBm and 0.929 % at -10 dBm, which corresponds to ambient RF power levels typically available in low-power scenarios. At 0 dBm, the PCE rises to 5.725 %, and at 10 dBm, the rectifier achieves 32.116 %, before reaching a maximum efficiency of 89.913 % at 17.5 dBm.

The results obtained are significant for two reasons. First, they confirm that the rectifier operates optimally at very low Pin levels, which is a critical requirement for practical IoT deployments where available RF energy is often below -10 dBm. Second, they reveal that the rectifier is able to scale its output effectively under stronger excitations, until it reaches a saturation point beyond 17.5 dBm, where additional increases in Pin result in negligible voltage improvement. The observed saturation around 16.4 V highlights both the efficiency and the practical operation limits of the design.

The proposed rectifier contributes significantly to this performance enhancement by boosting the output voltage, as previously discussed. While the inclusion of multiple diodes and capacitors inherently introduces conduction losses and slightly reduces efficiency at very low Pin levels, the design, however, ensures that the harvested energy remains usable. This trade-off between low PCE and high DC output voltage demonstrates the design's practical balance. Importantly, the ability to sustain measurable PCE even under weak input conditions confirms the circuit's suitability for RF-EH in environments where available RF power is scarce but still sufficient for intermittent or low-duty-cycle IoT applications.

Moreover, from a practical viewpoint, the proposed design can be readily fabricated using commercially available low-cost substrates such as Rogers or standard FR-4, depending on the desired balance between performance and cost. Rogers RT 5880 employed in this study offers low dielectric losses at high frequencies. However, FR-4 provides a more economical solution for large-scale IoT deployments, albeit with slightly reduced performance. The circuit relies on off-the-shelf Schottky diodes and surface-mount capacitors, which ensures ease of prototyping and scalability to industrial production without requiring complex CMOS fabrication.

ISSN No. 2454-6194 | DOI: 10.51584/IJRIAS |Volume X Issue IX September 2025

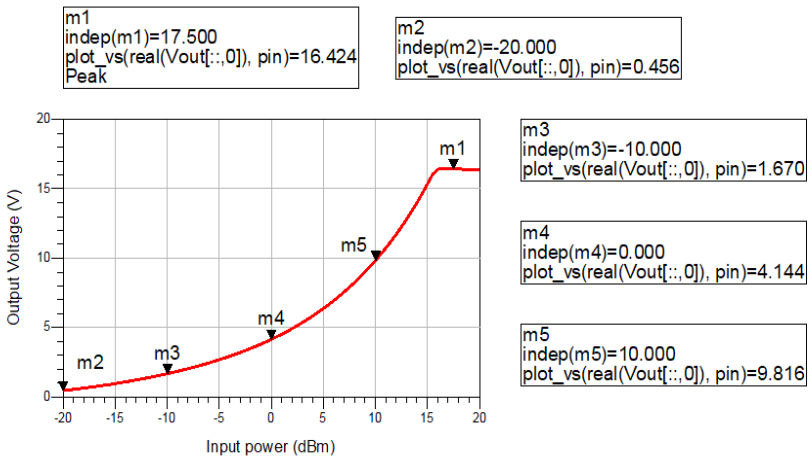

Figure 18. Pin Versus DC Output Voltage of Proposed 5-Stage CW Rectifier

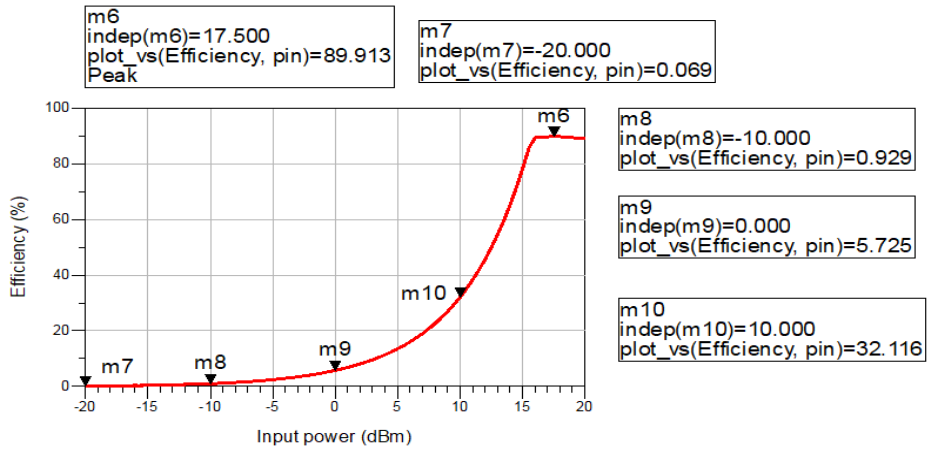

Figure 19. Pin Versus PCE of Proposed 5-Stage CW Rectifier

Comparative Analysis

The section provides a comparative analysis of the proposed RF-EH system against related works discussed in the literature review. The analysis is divided into two parts: the first assesses the performance of the receiver antenna, and the second evaluates the rectifier circuit. Table 2 compares the proposed 4x4 MPA array with the previously reported antenna designs, while Table 3 summarises the comparative performance of the proposed 5-stage rectifier.

Table 2 Comparison of Proposed 4x4 MPA Array with Existing Antenna Designs

SN	Reference	Frequency (GHz)	Substrate	Array Size	Return Loss (dB)	Gain (dBi)	Rad. Eff. (%)	Tot. Eff. (%)
1.	[9]	2.4, 5.8	FR-4	1x1	-14.104, -27.515	0.5102, 1.175	27, 38	25, 38
2.	[8]	2.4, 5.2	FR-4	1x2	-20.6, -16	1.6, 3.95	81, 80	69, 67
3.	[3]	1.83, 2, 2.45	Arlon	1x1	< -10	3.5, 5, 5	NA	NA
4.	[14]	1.8	FR-4	2x2	-25	9.2	NA	NA
5.	[15]	2.4	FR-4	1x2, 2x2, 2x3, 2x4	< -10	7.2, 11, 10.4, 10.3	NA	NA
6.	[7]	2.45	Rogers RT5880	3-element	-32.886	11.24	89.45	89.41
7.	[12]	2.3	FR-4	1x1, 2x2, 4x4	-15.4, -17.6, -17.10	3.05, 7.65, 13.05	NA	NA

8.	[16]	2.4	Rogers RT5880	7-element	< -50	15.8	96	94
9.	[17]	2.4	Rogers RO4003	2x4	-26.2	17.5	NA	NA
10.	This work	2.4	Rogers RT5880	4x4	-25.56	19.29	84.69	84.44

Table 3 Comparison of Proposed Five-Stage Rectifier with Existing Rectifier Designs

SN	Author (Year)	Frequency (GHz)	Diode Type	Input Power (dBm)	Number of Stages	Load Resistor (kΩ)	Maximum PCE (%)	Output Voltage (V)
1.	[18]	2.4	HSMS-2850	10	1	2	75	2.9
2.	[6]	2.45, 5.5	SMS7630 -061	-10	1	5	47, 27	0.51, 0.36
3.	[19]	2.45	HSMS-2850	19	1	20	77.57	1.092
4.	[20]	2.45	HSMS-2850	0	2	470	64	5.2
5.	[21]	2.45	HSMS-285C	20	7	1000	75	12
6.	This work	2.4	HSMS-2850	17.5	5	300	89.913	16.424

CONCLUSION

A 2.4 GHz RF-EH system was designed and optimised to provide a sustainable power solution for low-power IoT applications. This work focused on three key components: a high-gain 4x4 MPA array, an optimised single-stub MN and a cascaded 5-stage CW rectifier for efficient RF-to-DC conversion. The proposed 4x4 antenna array achieved a gain of 19.29 dBi and directivity of 20.01 dBi with radiation and total efficiencies exceeding 84 %, enabling effective RF signal capture. The single-stub MN achieved precise IM by transforming the rectifier's input impedance from (3.815 – j37.583) Ω to approximately 50 Ω, resulting in a return loss of -62.858 dB. This ensured minimal reflection and maximum PT between the antenna and rectifier. The cascaded 5-stage rectifier produced usable DC output voltages ranging from 0.456 V at -20 dBm to 4.144 V at 0 dBm, demonstrating strong suitability for IoT devices operating under limited RF availability. At higher input powers, the rectifier achieved a peak output voltage of 16.424 V with a PCE of 89.913 % at 17.5 dBm. Ultimately, the proposed RF-EH system provides a sustainable, cost-effective and eco-friendly power solution for large-scale IoT and Wireless Sensor Network (WSN) deployments, reducing the reliance on traditional batteries while ensuring efficient RF-to-DC power conversion. To further enhance system robustness, future work could explore hybrid energy harvesting approaches, where RF-EH is complemented with solar, thermal or vibration modalities. Such multi-source architectures would provide more reliable and sustainable power delivery, enabling support for more demanding IoT applications under diverse environmental conditions.

REFERENCE

1. Moloudian, G., Hosseinifard, M., Kumar, S., Simorangkir, R. B. V. B., Buckley, J. L., Song, C., Fantoni, G and O'Flynn, B. (2024), "RF Energy Harvesting Techniques for Battery-less Wireless Sensing, Industry 4.0 and Internet of Things: A Review", IEEE Sensors Journal, Vol. 24, No. 5, pp. 1 – 14.
2. Kanboz, B. and Palandöken, M. (2023), "Microstrip Patch Antenna Array Design for RF Energy Harvesting Applications", European Journal of Science and Technology, Vol. 3, No. 49, pp. 34 – 37.
3. Zeng, M., Li, Z., Ding, Y. and Lin, X. (2022), "A Wide-Band Antenna with Dual Open Rings Resonator for RF Energy Harvesting", Microwave and Optical Technology Letters, Vol. 64, No. 11, pp. 2019 – 2023.

4. Agrahari, R., Singh, S., Samantaray, D., Kumar, B., Bhattacharyya, S., Mahto, M. and Jain, P. K. (2023), "Triple-Band Meta-surface Absorber for RF Energy Harvesting Applications", Microwave and Optical Technology Letters, Vol. 65, No. 8, pp. 2252 – 2261.
5. Lee, Y. C., Ramiah, H., Choo, A., Churchill, K. K. P., Lai, N. S., Lim, C. C., Chen, Y., Mak, P. and Martins, R. P. (2023), "High-Performance Multiband Ambient RF Energy Harvesting Front-End System for Sustainable IoT Applications – A Review", IEEE Access, Vol. 11, No. 1, pp. 11143 – 11164.
6. Mehta, P. and Nella, A. (2024), "Dual-Band Low-Power RF-to-DC Signal Converter Circuits for Energy Harvesting", AIP Advances, Vol. 14, No. 7, pp. 1 – 13.
7. Ansah, J. N. and Annan, J. K. (2024), "A Novel Triangular Configuration of a Rectangular Patch Antenna Array For 2.45 GHz RF Energy Harvesting", International Research Journal of Engineering and Technology, Vol. 11, No. 11, pp. 420 – 427.
8. El-Issawi, M. L., Konditi, D. B. O. and Usman, A. D. (2024), "Design of an Enhance Dual-Band Microstrip Patch Antenna with Defected Ground Structures for WLAN and WiMAX", Indonesian Journal of Electrical Engineering and Computer Science, Vol. 35, No. 1, pp. 165 – 174.
9. Küçükcan, S. and Kaya, A. (2022), "Dual-Band Microstrip Patch Antenna Design for Wi-Fi Applications", European Journal of Science and Technology, Vol. 2, No. 34, pp. 661 – 664.
10. Luo, Y., Pu, L., Wang, G. and Zhao, Y. (2019), "RF Energy Harvesting Wireless Communications: RF Environment, Device Hardware and Practical Issues", Sensors, Vol. 19, No. 13, 3010pp.
11. Huang, Y. and Boyle, K. (2008), Antennas: From Theory to Practice, John Wiley and Sons Ltd, Chichester, United Kingdom, (ed.), 2nd Edition, pp. 1 – 363.
12. Wijayanti, A., Putri, T. L., Puspitorini, O. and Siswandari, N. A. (2024), "Design of Microstrip Planar Array Antenna for Wireless Sensor Device Charging at Frequency 2300 MHz", Proceedings of the International Conference on Applied Science and Technology on Engineering Science 2023 (iCAST-ES 2023), Dordrecht, Netherlands, pp. 493–505.
13. Kuşin, Y. E. and Palandöken, M. (2023), "Machine Learning Based B-Shaped Monopole Antenna for RF Energy Harvesting Applications", International Journal of Advanced Natural Sciences and Engineering Researches, Vol. 7, No. 2, pp. 1 – 8.
14. Sharma, T. and Saini, G. (2016), "Microstrip Antenna Array for RF Energy Harvesting System", International Journal of Advanced Information Science and Technology, Vol. 45, No. 45, pp. 145 – 149.
15. Jayanthy, T., Harini, J., Haseena, A. and Neha, C. L. (2024), "Design and Analysis of Triangular Patch Antenna Array", International Journal of Engineering Applied Sciences and Technology, Vol. 8, No. 12, pp. 123 – 128.
16. Kabeel, A. A., Hussein, A. H., ElMaghrabi, A. E. and Elabd, R. H. (2023), "Design of a Circular Concentric Microstrip Patch Antenna Array for Wi-Fi Band Energy Harvesting", Journal of Engineering Research, Vol. 7, No. 5, pp. 156 – 159.
17. Nnamdi, U., Omijeh, B. and Asianuba, I. (2023), "Design and Optimisation of a 2.4 GHz Antenna Array for Energy Harvesting", European Journal of Theoretical and Applied Sciences, Vol. 1, No. 6, pp. 676 – 683.
18. Subbyal, H., Ali, W. and Liguo, S. (2022), "Compact Antenna Integrated with a Greinacher Voltage Multiplier for Ambient Energy Harvesting Applications", International Journal of RF and Microwave Computer-Aided Engineering, Vol. 32, No. 12, pp. 1 – 10.
19. Pramono, S., Shidiq, D. D., Ibrahim, M. H., Adriyanto, F. and Hikmaturokhman, A. (2021), "RF Energy Harvesting using a Compact Rectenna with an Antenna Array at 2.45 GHz for IoT Applications", Journal of Electrical Engineering, Vol. 72, No. 3, pp. 159 – 167.
20. Khan, N. U., Ullah, S., Khan, F. U. and Merla, A. (2024), "Development of 2400-2450 MHz Frequency Band RF Energy Harvesting System for Low-Power Device Operation", Sensors, Vol. 24, No. 10, pp. 1 – 13.
21. Omara, F. A., Ali, W. A. E., Eltrass, A. S. and Abbasy, N. H. (2024), "Design of a 2.45 GHz Rectenna Based on High-Gain 2-Element Array Antenna and 7-stage Voltage-Doubler Rectifier for Energy Harvesting Applications", Physica Scripta, Vol. 99, No. 12, pp. 1 – 20.

ISSN No. 2454-6194 | DOI: 10.51584/IJRIAS |Volume X Issue IX September 2025

APPENDIX A

Table A1. Dimensions of the 4x4 MPA Array

Parameter	Value (mm)	Parameter	Value (mm)
Ws	400	Ls	360
Wg	400	Lg	360
Wp	51	Lp	42.35
Wmf	4.89	Lmf	200
Wif	8.90	Lif	10
Wtj_1	30	Ltj_1	1.42
Wq_1	20	Lq_1	2.81
Wc_1	20	Lc_1	4.89
Wpf	4.89	Lpf	20
Wtj_2	1.42	Ltj_2	20
Wq_2	2.81	Lq_2	15
Wc_2	4.89	Lc_2	15
Wtj_3	130	Ltj_3	1.42
Wq_3	20	Lq_3	2.81
Wca_3	15	Lca_3	4.89
Wcb_3	4.89	Lcb_3	26
Wtj_4	1.42	Ltj_4	85
Wq_4	2.81	Lq_4	20
Wc_4	4.89	Lc_4	20
d	110		